

## Research Paper

# Assessment of heat mitigation capacity of urban greenspaces with the use of InVEST urban cooling model, verified with day-time land surface temperature data



J.E. Zawadzka<sup>\*</sup>, J.A. Harris, R. Corstanje

Centre for Environmental and Agricultural Informatics, School of Water, Energy and Environment, Cranfield University, Bedfordshire, UK

## HIGHLIGHTS

- InVEST Urban Cooling model was validated with day-time land surface temperature data.
- Heat mitigation index adequately approximates LST at 30 m resolution.
- The index is sensitive to cooling distance and spatial resolution of the analysis.
- InVEST Urban Cooling model can support decisions at masterplan level.

## ARTICLE INFO

**Keywords:**  
InVEST Urban Cooling model  
Urban heat island  
Temperature regulation  
Heat mitigation  
Land surface temperature

## ABSTRACT

Accurate quantification of the heat mitigation capacity of urban greenspaces is essential in planning decisions due to increased thermal pressures on existing and new urban environments associated with climate change. However, this often requires data analytical skillsets that may not be available to the planning community. The recently developed InVEST 3.8.7 Urban Cooling model addresses this limitation by using several easily accessible parameters, assigned to a land cover map, to produce a heat mitigation index (HMI) intended to estimate the cooling capacity of vegetation in a spatial context. In this study, we validated the HMI derived for three towns with differing morphologies by comparison to land surface temperature (LST) data using linear regression analysis. We found that the HMI can be used to explain a variable proportion of the variation in LST, with  $R^2$  ranging from 0.48 to 0.64 depending on the town, with stronger associations obtained for towns with a higher range of LST values. Higher resemblance to LST data was achieved after resampling of the 2 m resolution model outputs to 30 m resolution, inclusion of water bodies as cooling features, and using cooling distance away from large greenspaces of 100 m. On average, a change in the HMI of 0.1 was associated with 0.76 °C change in LST. We conclude that the model is suitable for assessment of heat mitigation interventions through incorporation of vegetation and water bodies into city plans at scales relevant to masterplans rather than fine-tuning of urban design.

## 1. Introduction

Urban areas are affected by the urban heat island (UHI) effect, whereby ambient temperatures of towns and cities are generally warmer than in the surrounding rural environments (Oke, 1976). The UHI effect is associated with detrimental effects on human health (e.g. Heaviside, Macintyre, & Vardoulakis, 2017; Heaviside, Vardoulakis, & Cai, 2016), increased energy consumption for air conditioning (Santamouris, Cartalis, Synnefa, & Kolokotsa, 2015), increased occupational heat stress

(Casanueva et al., 2020; Kjellstrom, Freyberg, Lemke, Otto, & Briggs, 2018), and changes to ecological cycles (Yow, 2007). Moreover, maintaining thermal comfort of urban inhabitants within public spaces has been proven essential for stimulation of physical activity and public life within cities (Elliott, Eon, & Breadsell, 2020). The incidence of heat-waves is expected to rise in frequency and intensity this century (Perkins, Alexander, & Nairn, 2012; Wouters et al., 2017), which, together with the anticipated growth of urban inhabitants to 68% of global population by year 2050 (United Nations, Department of Economic, &

\* Corresponding author at: MK43 0AL Bedfordshire, UK.

E-mail address: [joanna.zawadzka@cranfield.ac.uk](mailto:joanna.zawadzka@cranfield.ac.uk) (J.E. Zawadzka).

Social Affairs, 2019), highlight the need for rapid implementation of heat mitigation measures across cities in order to avoid or reduce their negative impacts.

The urban thermal environment is often described in the context of the formation of the UHI or surface urban heat islands (SUHI). The UHI is a phenomenon originally conceived as occurring at night, moderated through radiative fluxes of sensible and latent heat, the former characteristic of the urban built environment and associated with increased air temperatures and the latter – of vegetated surfaces, associated with cooling properties (Lin, Gou, Lau, & Qin, 2017; Oke, 1988). The formation and intensity of the UHI effect is governed by complex interactions between multiple factors that include decreased long-wave radiation loss from and multiple reflections of short-wave radiation between buildings, increased storage of sensible heat in the urban fabric, decreased evapotranspiration due to low vegetation coverage as compared to rural areas, anthropogenic heat sources, and air pollution (Oke, Johnson, Steyn, & Watson, 1991). The SUHI relates to the temperature of the urban land surface and is associated with the UHI through modulation of air temperature at the lowest layers of the atmosphere (Voogt & Oke, 2003), however, with differences induced through air advection (Wang, Yao, & Shu, 2020), and being more prominent during the day (Roth, Oke, & Emery, 1989).

In urban planning, excess heat mitigation is primarily concerned with regulation of microclimates at pedestrian or building scales (Erell, 2008) that could be related to the street or site (micro-scale) levels (Norton et al., 2015). Whilst pedestrian scales mostly relate to the creation of outdoor spaces providing thermal comfort to humans, building scales focus on measures leading to energy conservation in buildings. Multiple typologies of (S)UHI mitigation methods exist (Aleksandrowicz, Vuckovic, Kiesel, & Mahdavi, 2017; Kleerekoper, van Esch, & Salcedo, 2012; Meng, 2017; Sung, 2013), and include introduction of strategically distributed vegetation and water bodies across the landscape, termed green and blue infrastructure (European Commission, 2013; Gunawardena, Wells, & Kershaw, 2017), which reduce surface and air temperatures through shading, evapotranspiration, and evaporation. These effects are detectable at a distance away, both in the case of air as well as surface temperatures (Aram, Higueras García, Solgi, & Mansournia, 2019), with distances dependant on specific morphologies of the neighbourhoods, among other factors. Incorporation of green infrastructure as a (S)UHI mitigation measure into urban plans generates an opportunity to introduce ecosystem services, i.e. benefits humans derive from nature (Millennium Ecosystem Assessment, 2005), other than local temperature regulation into the urban landscapes, which requires assessment of benefits derived from them, both in biophysical and economic terms (Cortinovis & Geneletti, 2019).

Biophysical assessments of heat mitigation capacity of vegetation can be carried out through air temperature measurements (Bowler, Buyung-Ali, Knight, & Pullin, 2010), analysis of remotely sensed land surface temperature (LST) imagery (Zhou et al., 2019), or simulations of urban thermal environment (Tsoka, Tsikaloudaki, Theodosiou, & Bikas, 2020) – approaches that require substantial academic expertise that is rarely available in many planning departments (Bherwani, Singh, & Kumar, 2020; Norton et al., 2015). An example of a recently developed model dedicated to a simplified assessment of the UHI mitigation capacity of vegetation, which has a potential to bridge this gap, is the Urban Cooling model available from a wider suite of ecosystem services modelling tools called InVEST (Integrated Valuation of Ecosystem Services and Trade-offs) developed by the Natural Capital Project (Sharp et al., 2020). InVEST comprises a suite of spatially-explicit ecosystem services models covering terrestrial, freshwater, marine and coastal ecosystems that are aimed at the assessment of synergies and trade-offs between different management options of natural resources leading to the determination of areas where investment can enhance both human development and environmental conservation.

The Urban Cooling model calculates the heat mitigation index (HMI) based on evapotranspiration from vegetation, cooling distance of large

urban parks, and albedo assigned to a land cover (LC) map, which is then used to estimate average cooling capacity on air temperature and monetary value associated with the vegetative cooling, and as such is the key model output determining the accuracy of subsequent evaluations. Consequently, the goal of this study was to validate the representativeness of the HMI returned by the InVEST 3.8.7 Urban Cooling model of urban thermal environment as depicted by LST imagery captured on a warm summer day, at spatial resolutions relevant to micro- and broad-scale assessments: 2 and 30 m. We therefore hypothesised that the HMI generated by the InVEST 3.8.7 Urban Cooling model can be used as a substitute for LST mapping in assessment of the cooling capacity of urban greenspaces under an assumption that low HMI values should correspond to highest temperatures in the LST image with the opposite being true for the high values of HMI. We next estimated the amount of change in LST due to gradual change in the HMI for model outputs with the highest resemblance to the LST data as indicated by the highest value of  $R^2$ . Our analysis was carried out using an example of three sub-urban towns collectively characterised with a high variety of urban form, and is one of the first studies aiming at validation of the InVEST 3.8.7 Urban Cooling model.

## 2. Materials and methods

### 2.1. Study area

The study area comprises three towns located in a relatively close proximity in England: Milton Keynes ( $52^{\circ}0'N$ ,  $0^{\circ}47'W$ , appr.  $122\text{ km}^2$ ), Bedford ( $52^{\circ}8'N$ ,  $0^{\circ}27'W$ , appr.  $60\text{ km}^2$ ), and Luton/Dunstable ( $51^{\circ}52'N$ ,  $0^{\circ}25'W$ , appr.  $86\text{ km}^2$ ) (Fig. 1) with population of 229,941, 106,940, and 258,018 (Office for National Statistics, 2013) respectively and a temperate oceanic climate according to the Köppen–Geiger climate classification system with the highest monthly average air temperatures of approximately  $22^{\circ}\text{C}$  in July and lowest temperatures of approximately  $1^{\circ}\text{C}$  observed in February, and the average annual precipitation of 598, 657, and 712 mm for Bedford, Milton Keynes and Luton respectively. The three towns are characterised with contrasting histories: modern-day garden-city, medieval, and industrial, respectively, collectively representing a wide range of urban form patterns representative of British towns (Grafius et al. 2016) and allowing for evaluation of Urban Cooling model's performance in towns with various morphologies. Milton Keynes is a recently designed Garden City abundant in parks, greenspaces and water bodies, characterised by a grid of dual-carriageways dissecting the town into clearly defined neighbourhoods. Bedford is a medieval market town characterised with densely built-up city centre with several parks and residential areas located at the outskirts. Luton, on the other hand, is an industrial-era town characterised with a modern densely built-up city centre and residential areas composed of terraced housing.

The differing histories and urban form patterns of the three towns reflect on their land cover distribution (Table 1). Major differences in LC composition of the towns, as assessed from the high-resolution land cover maps available in this study and described in more detail in Section 2.2.2, comprise the lowest abundance of greenspaces and the highest of impervious areas in Luton, and the largest extent of greenspaces and water bodies in Milton Keynes.

### 2.2. Materials and methods

The following sections explain the main assumptions of the InVEST 3.8.7 Urban Cooling model leading to the generation of raster maps of the heat mitigation index (HMI) as well as steps undertaken to assess the strength of the relationship between the HMI and land surface temperature data available for the three towns. The map of the HMI is the key output of the model from which tabular estimates of average cooling capacity, average air temperature and air temperature anomaly together with the value of the heat reduction services by urban green

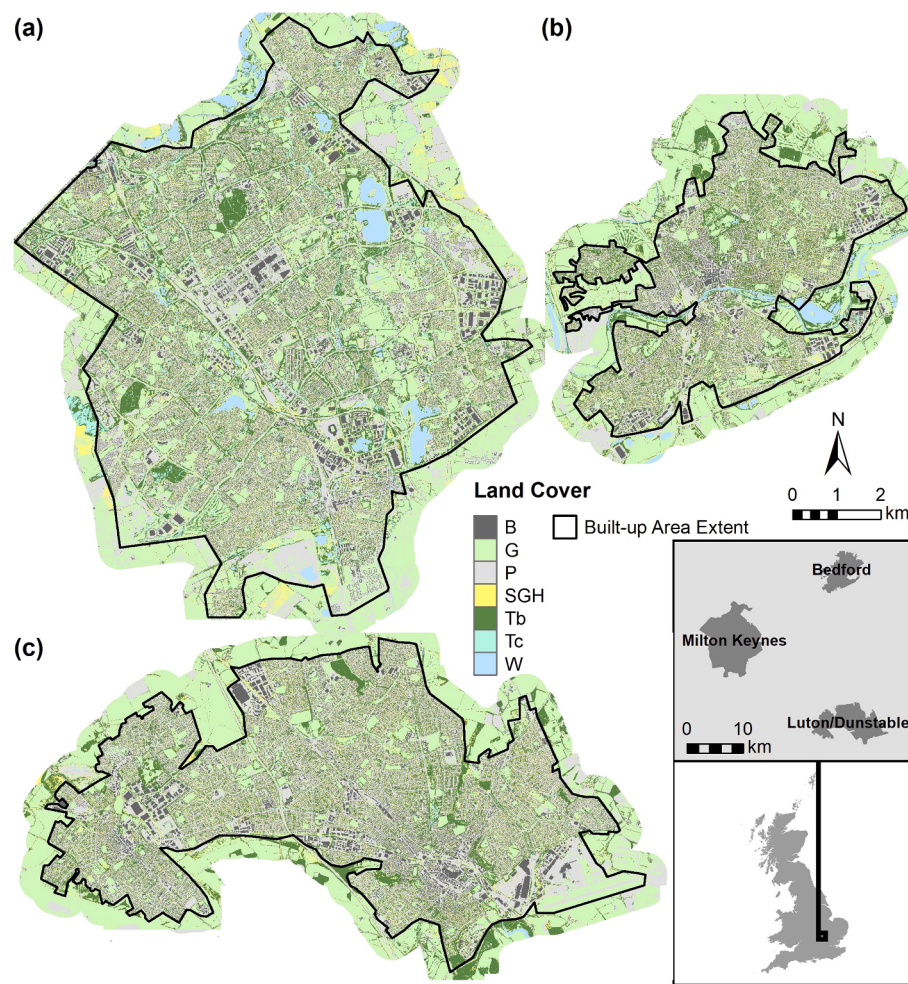


**Fig. 1.** Land cover in (a) – Milton Keynes, (b) – Bedford, (c) – Luton/Dunstable. The insert depicts location of the towns within Great Britain. B – buildings, G – grass, P – paved, SGH – short trees/tall grass/hedge, Tb – broadleaf trees, Tc – coniferous trees, W – water.

**Table 1**

Land cover composition and patch size (mean and standard deviation) of main land cover types within Bedford (BD), Luton (LT) and Milton Keynes (MK) summarised for the built-up area extents of the towns from the land cover maps available in this study.

LC	LC area [% of total town area]			Patch size [m <sup>2</sup> ]					
	BD	LT	MK	BD		LT		MK	
				Mean	Std.	Mean	Std.	Mean	Std.
Buildings	B	18.8	16.1	12.1		160	529	154	918
Grass - Short < 0.5 m	G	28.4	21.3	28.5		49	823	48	1108
Shrub/Tall Grass/Hedge (0.5–2 m)	SGH	9.9	7.7	7.7		13	24	13	26
Broadleaf Trees > 2 m tall	Tb	24.7	18.0	22.7		49	462	52	935
Coniferous Trees > 2 m tall	Tc	0.3	N/A	4.0		84	255	N/A	N/A
Paved	P	35.6	36.8	34.1		122	7648	156	45,672
Water	W	1.2	0.1	3.0		283	2115	96	432
								124	44,987
								640	9899

infrastructure are derived by the model.

### 2.2.1. InVEST urban cooling model

The InVEST 3.8.7 Urban Cooling model generates maps of the heat mitigation index (HMI) that estimates the cooling capacity of urban greenspaces on all LC classes present in the study area by taking into account the cooling capacity of larger urban parks extending beyond their boundaries (InVEST 3.8.7 User Guide). The functionality of the model is based on and expands upon the methodology for the estimation of cooling capacity of urban green infrastructure, encompassing LC features such as grass, trees, green walls/roofs and water, in the planning context proposed by Zardo et al. (2017).

In the Urban Cooling model, cooling capacity (CC) is calculated as a weighted function of shading (S), evapotranspiration index (ETI) and albedo (A) (Equation 1), the latter constituting an extension to the method presented by Zardo et al. (2017). Albedo expresses the proportion of solar radiation reflected by land surface, and is therefore representative of the amount of solar heat than can be absorbed by surface materials, with lower absorption, i.e. higher albedo, associated with lower land surface temperature (Phelan et al., 2015).

$$CC = 0.6 \cdot S + 0.2 \cdot ETI + 0.2 \cdot A \quad (1)$$

where: CC – cooling capacity index, ranging from 0 to 1, with 0 as no

cooling capacity, and 1 maximum cooling capacity within the study area, S – capacity of trees to provide shading, set to 1 for trees taller than 2 m or 0 for trees below the 2 m cut-off,

ETI – evapotranspiration index, calculated from Equation 2, A – albedo, ranging from 0 to 1, with 1 indicating maximum reflectance of solar radiation, and 0 – maximum absorption.

ETI is the normalised value of evapotranspiration across the study area calculated as actual evapotranspiration ( $ET_a$ ) divided by the maximum value of  $ET_0$  within the study area ( $ET_{max}$ ) (Equation 2).  $ET_a$  is calculated as potential evapotranspiration  $ET_0$  modified by the value of crop coefficient  $K_c$  determining the fraction of  $ET_0$  evaporated by specific type of land cover (Equation 3).

$$ETI = \frac{ET_a}{ET_{max}} \quad (2)$$

$$ET_a = ET_0 \cdot K_c \quad (3)$$

Potential evapotranspiration  $ET_0$  was calculated from the modified Hargreaves equation (Equation 4) (Droogers & Allen, 2002).

$$ET_0 = 0.0013 \cdot 0.408 \cdot RA \cdot (T_{avg} + 17) \cdot (TD - 0.0123 \cdot P)^{0.76} \quad (4)$$

where:  $ET_0$  – reference evapotranspiration, [ $\text{mm d}^{-1}$ ], RA – extra-terrestrial radiation, estimated as  $41.6 \text{ MJ m}^{-2}\text{d}^{-1}$ , equivalent to RA of the 15th day of June at  $52^\circ\text{N}$  in Allen et al. (1998), P – Precipitation [mm],  $T_{avg}$  – the average of the daily minimum and daily maximum temperatures [ $^\circ\text{C}$ ], TD – the difference between daily maximum and mean daily minimum temperatures [ $^\circ\text{C}$ ].

The HMI is equivalent to cooling capacity derived for each grid cell of the land cover map submitted to the model based on several conditions. These conditions distinguish between grid cell location within a large greenspace (over 2 ha in size), location within a cooling distance away from large greenspaces, and location outside of the cooling zone of influence, indicated by the cooling distance, of large greenspaces on temperature (Equation 5).

$$HMI_i = \begin{cases} CC_i & \text{if } CC_i \geq CC_{Park_i} \text{ or } GA_i < 2\text{ha} \\ CC_{Park_i} & \text{otherwise} \end{cases} \quad (5)$$

where:  $HMI_i$  – heat mitigation index value at grid cell  $i$ ,  $CC_i$  – cooling capacity of grid cell  $i$ , calculated from Equation 1,  $CC_{Park_i}$  – cooling capacity calculated as distance weighted average of the CC values from green spaces (Equation 7),  $GA_i$  – the amount of green areas within a search distance  $d_{cool}$  around each pixel (Equation 6).

$$GA_i = cell_{area} \cdot \sum_{\substack{j \in dradius \\ from i}} g_j \quad (6)$$

where:  $GA_i$  – the amount of greenspaces around grid cell  $i$  within a radius defined by cooling distance  $d_{cool}$ ,  $cell_{area}$  – area of grid cells  $j$  within the input raster land cover map, expressed in hectares,  $g_j$  – a switch assuming the value of 1 if a grid cell located within the cooling distance radius represents greenspaces, otherwise set to 0.

$$CC_{Park_i} = \sum_{\substack{j \in dradius \\ from i}} g_j \cdot CC_j \cdot e^{\left(\frac{-d(i,j)}{d_{cool}}\right)} \quad (7)$$

where:  $CC_{Park_i}$  – cooling capacity assigned to areas located within the cooling distance radius  $d_{cool}$  from large greenspaces ( $>2\text{ha}$  in size), calculated as the weighted average of the distance between cells  $i$  and  $j$ ,  $d(i,j)$  – distance between cells  $i$  and  $j$  located within the cooling distance radius.

The Urban Cooling model can also be used to estimate night-time heat mitigation for buildings, air temperature anomalies as well as economic value of heat mitigation by urban greenspaces, however, these

functions are derivative from the HMI and are not covered in this study.

## 2.2.2. Model parameterisation and data sources

The primary input required by the InVEST 3.8.7 Urban Cooling model is a land use/land cover map, classes of which are attributed with parameters required for the calculation of the HMI. In this study, a 2 m spatial resolution LC map in a raster format was used. The map was collated for the purpose of previous studies (Grafius, Corstanje, Siriwardena, Plummer, & Harris, 2017; Grafius et al., 2016, 2019) from three datasets: NDVI-derived locations of grass and trees generated from colour-infrared aerial photography at 0.5 m spatial resolution available from LandMap Spatial Discovery project (<http://learningzone.rspoc.org.uk/>) and captured between 2007 and 2010, footprints of buildings and paved areas captured by a large-scale topographic map (Ordnance Survey MasterMap with the latest updates applied in December 2011), and feature heights acquired from a LiDAR data survey of the three towns in 2012. The parameters assigned to each LC class include potential evapotranspiration  $ET_0$ , evapotranspiration coefficient ( $K_c$ ), albedo, cooling distance away from large greenspaces, as well as greenspace and shading switches (Table 2). Precipitation and temperature data needed for the  $ET_0$  estimation were obtained from the HadUK-Grid Gridded Climate Observations on a 1 km grid over the UK (Hollis, McCarthy, Kendon, Legg, & Simpson, 2019) for 8 June 2013 and calculated as a mean value for each town. Evapotranspiration coefficients assigned to the main LC classes present in the study area were approximated from existing guidance on crop evapotranspiration calculation (Allen et al., 1998) whose use is advised by the InVEST User Guide. In all cases, mid-season values of  $K_c$  were selected, which aligned well with well-developed vegetation in the three towns in early June.  $K_c$  for grass, coniferous trees and water could directly be estimated from the guidance as values for turf grass, coniferous trees and temperate climate water bodies respectively. The guidance did not include the evapotranspiration coefficient for broadleaved trees and therefore it was approximated by  $K_c$  for apple orchards without ground cover, which was deemed appropriate due to the very high resolution of the LC map available in this study capable of depicting single trees without their surrounding land cover. Buildings and paved areas were assigned a very small value of  $K_c$  (0.001) to avoid creation of empty grid cells in the intermediary outputs of the model – a setting recommended for other models included in the InVEST tool, such as the Seasonal Water Yield model. Albedo values for each LC class were estimated from the list of typical values in Taha et al. (1988), assuming highest absorption of solar radiation by water followed by paved areas due to dark colour of asphalt roads, and lowest for buildings, with vegetated areas taking intermediary values. Following the methodology for cooling capacity estimation presented by Zardo et al. (2017) that included evaporative cooling of water bodies as well as vegetation, the greenspace switch was assigned not only to grassed and treed LC classes but also water, resulting with model runs capturing cooling capacity of vegetation only (V) or water and vegetation (W&V) (Fig. 2). Three cooling distances away from large greenspaces were considered: 100 m, 200 m, and 300 m, which

**Table 2**

Key parameters assigned to each land cover class within the study area submitted to the model as the biophysical table.\*Separate runs of the model were carried out where water was treated as the greenspace to include its evaporative cooling capacity in the calculation of the HMIx for each town.

LC	Description	Shade	$K_c$	Albedo	Greenspace
B	Buildings	0	0.001	0.25	0
G	Grass - Short $< 0.5 \text{ m}$	0	0.95	0.16	1
SGH	Shrub/Tall Grass/Hedge (0.5–2 m)	0	0.95	0.18	1
Tb	Broadleaf Trees $> 2 \text{ m}$ tall	1	0.95	0.2	1
Tc	Coniferous Trees $> 2 \text{ m}$ tall	1	1	0.15	1
P	Paved	0	0.001	0.14	0
W	Water	0	0.6525	0.09	0 or 1*

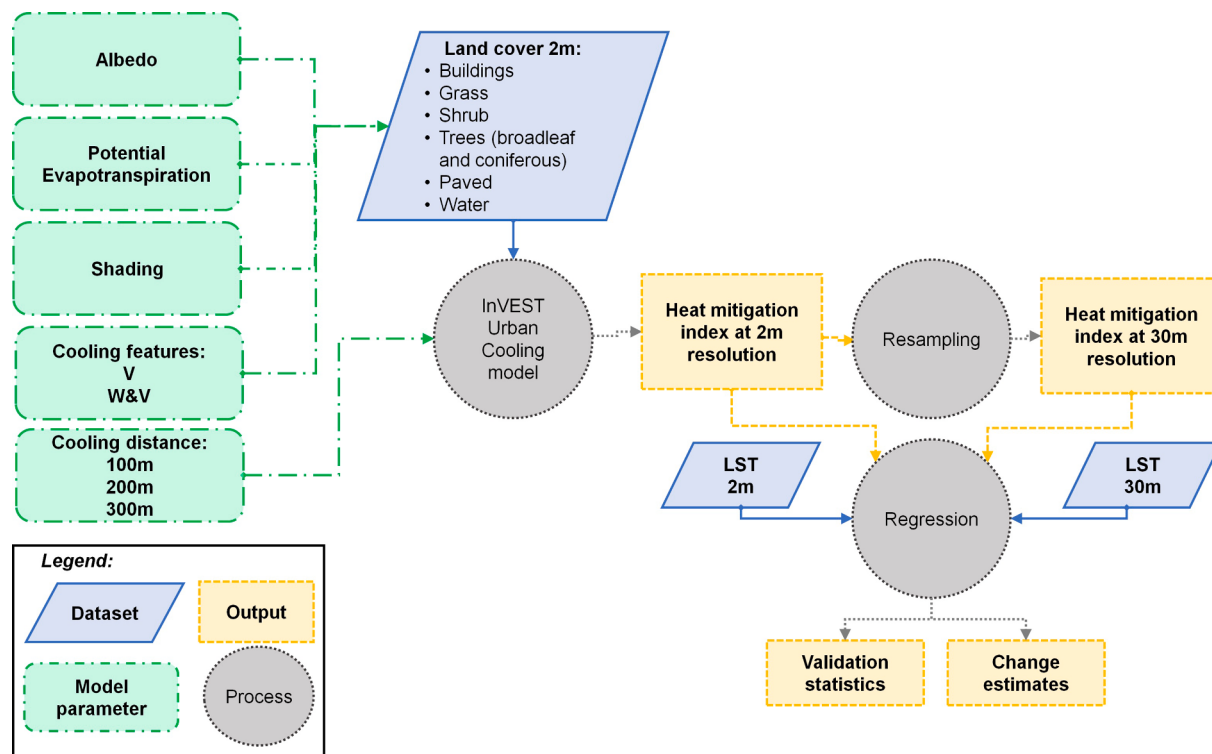


**Fig. 2.** Schematic of the methodology undertaken to assess the representativeness of the heat mitigation index derived from land cover maps with different cooling distance and cooling features settings in relation to land surface temperature (LST). V – vegetation, W – water.

approximated distances reported in literature regarding the cooling capacity of urban parks, ranging between 20 and 440 m (Aram et al., 2019; Vaz Monteiro, Doick, Handley, & Peace, 2016).

Additional settings required by the model included the air temperature reference value and the UHI magnitude, which were set to the minimum air temperature observed within a 10 km radius away from each town and the difference between maximum air temperature value within each town and the reference value, all captured from the HadUK-Grid Gridded Climate Observations on a 1 km grid over the UK (MetOffice, 2019) dataset. Air mixing distance was kept as the default value of 2000 m. Whilst these settings were required for the model to run, they did not affect the HMI values returned by the model that are subject of this study.

### 2.2.3. Verification of model outputs

The heat mitigation maps obtained from InVEST 3.8.7 Urban Cooling model were compared to LST data available for 8 June 2013 for the three towns. LST maps were available at two spatial resolutions: 2(4)m and 30 (100)m, for simplicity referred to as 2 and 30 m throughout the manuscript. The coarser resolution LST image was obtained from Landsat 8 thermal infra-red bands using split-window algorithm (Jimenez-Munoz, Sobrino, Skokovic, Mattar, & Cristobal, 2014). Its mixed spatial resolution stems from the fact that the Landsat 8 thermal infra-red data are captured at 100 m resolution and are subsequently resampled to 30 m resolution by the data provider (USGS). The finer resolution image was generated from the Landsat 8 LST map through a downscaling procedure (Zawadzka et al., 2020) whereby coarse resolution LST was related through a multivariate adaptive regression splines algorithm to spectral indices at 2 and 4 m resolution to produce the fine resolution images across the three towns.

The comparison between the HMI and LST data was carried out with the use of the ordinary least squares (OLS) linear regression for the area encompassed within the built-up area boundary (Fig. 1) that was manually digitised from aerial imagery used to generate the LC maps available in this study and representing a distinction between areas

considered as urban and the rural background of fields and pastures. Whilst the HMI maps that were generated at 2 m resolution by the model could directly be compared to the 2(4)m resolution LST images, the comparison to 30(100)m LST data required that the HMI datasets were resampled to match the mixed spatial resolution of the satellite-derived LST maps. This was done through the reproduction of the post-processing procedure for the Landsat 8 TIR bands captured by the sensor at 100 m resolution by first upscaling of the 2 m HMI to 100 m using a mean function within a 100 m x100m focal moving window and subsequent resampling, using the cubic convolution method, to 30(100) m with GIS procedures implemented in ESRI ArcGIS 10.6. Resampling of the 2 m resolution HMI maps to 30 m resolution allowed for direct comparisons with 30(100)m resolution LST datasets using linear regression as both maps carried signals of thermal response of all land cover types present within the coarse-resolution pixels without the need for multiple regression accounting for each land cover type located within the pixels. Ultimately, twelve HMI maps were generated for each town, accommodating for three different cooling distances away from large vegetated patches: 100, 200, and 300 m; two sets of cooling features: V or W&V; and two spatial resolutions of the outputs: 2 and 30 m.

## 3. Results

### 3.1. Validation with LST data

#### 3.1.1. City-wide assessment

Ordinary least squares regression analysis between spatially distributed values of the HMI index and LST revealed that the Urban Cooling model managed to reflect some portion of variation in thermal response of the land surface, however, the strength of the association depended on various factors considered in this study (Table 3 and Fig. 3). The largest differences in the coefficient of determination  $R^2$  were observed for regressions at different spatial resolutions, with associations between datasets at 30 m being at least twice as strong as at 2 m in Bedford and Luton, however, very similar in Milton Keynes. Whilst

**Table 3**

The outcomes of linear regression between HMI and LST data for three towns (Bedford – BD, Luton – LT and Milton Keynes – MK) between HM index and LST obtained at various spatial resolutions, cooling distances and cooling features (V – Vegetation, W&V – water and vegetation) settings. All coefficients were statistically significant at p value of 0.

Town	Cooling distance	Cooling features	Rsq		adj Rsq		Std Error		Intercept a		Coefficient b		Std Error a		Std Error b	
			2 m	30 m	2 m	30 m	2 m	30 m	2 m	30 m	2 m	30 m	2 m	30 m	2 m	30 m
BD	100 m	V	0.24	0.48	0.24	0.48	1.75	2.29	31.45	32.28	-2.87	-7.29	0.00	0.02	0.00	0.03
		W&V	0.28	0.63	0.28	0.63	1.71	1.94	31.56	32.97	-3.08	-8.05	0.00	0.02	0.00	0.03
	200 m	V	0.16	0.44	0.16	0.44	1.84	2.37	33.81	38.61	-5.48	-14.86	0.00	0.05	0.00	0.07
		W&V	0.18	0.59	0.18	0.59	1.81	2.03	34.21	40.59	-5.99	-17.11	0.00	0.04	0.00	0.06
LT	100 m	V	0.12	0.46	0.12	0.46	1.88	2.34	33.88	41.54	-5.47	-19.11	0.00	0.06	0.01	0.09
		W&V	0.14	0.58	0.14	0.58	1.86	2.05	34.39	43.86	-6.13	-21.71	0.00	0.06	0.01	0.08
	200 m	V	0.24	0.64	0.24	0.64	1.59	1.84	31.70	32.19	-2.81	-7.86	0.00	0.01	0.00	0.02
		W&V	0.25	0.64	0.25	0.64	1.58	1.83	31.70	32.20	-2.83	-7.85	0.00	0.01	0.00	0.02
MK	300 m	V	0.19	0.63	0.19	0.63	1.64	1.87	33.42	37.87	-4.60	-14.66	0.00	0.03	0.00	0.04
		W&V	0.19	0.63	0.19	0.63	1.64	1.87	33.44	37.87	-4.63	-14.63	0.00	0.03	0.00	0.04
	100 m	V	0.14	0.63	0.14	0.63	1.70	1.85	33.47	40.67	-4.54	-19.06	0.00	0.03	0.00	0.05
		W&V	0.14	0.63	0.14	0.63	1.70	1.85	33.50	40.69	-4.58	-19.06	0.00	0.03	0.00	0.05
MK	200 m	V	0.22	0.22	0.22	0.22	1.67	2.44	31.60	34.09	-6.06	-11.53	0.00	0.04	0.00	0.06
		W&V	0.24	0.44	0.24	0.44	1.64	2.07	31.93	37.18	-6.42	-15.69	0.00	0.03	0.00	0.05
	300 m	V	0.18	0.26	0.18	0.26	1.71	2.39	31.79	37.56	-6.28	-16.83	0.00	0.05	0.00	0.08
		W&V	0.20	0.45	0.20	0.45	1.69	2.06	32.21	40.68	-6.76	-20.85	0.00	0.04	0.00	0.06

the generally higher  $R^2$  values at 30 m resolution could be attributed to the introduction of a greater variance of values into the HMI maps during resampling from 2 m to 30 m resolution, the different behaviour in Milton Keynes could potentially be caused by the distinct morphology of this town, being designed as a Garden City and consequently containing distinctly larger patches of grass, trees and water than the remaining towns.

In all towns, the cooling distance of 100 m resulted in higher  $R^2$  values, however, inclusion of water bodies as cooling features had a varied effect on the strength of associations between the HMI and LST. The highest increase in  $R^2$  values was observed in Milton Keynes, followed by Bedford, and no increase was observed in Luton, which can be explained by the decreasing proportion of water in LC of these cities, respectively. Whilst the changes in  $R^2$  are only marginal at 2 m resolution, they are distinct for data at 30 m resolution, which could be attributed to the increased variance of HMI values resulting from the resampling.

The HMI values derived at 100 m cooling distance were distinctly lower than for the distances of 200 m or 300 m tested here (Tables 1 and 2, [Supplementary Materials](#)). Although increasing HMI values with increasing cooling distances of large greenspaces is expected, the difference observed in our study stems also from the fact that the cooling distance parameter set within the model by the user is also used to determine the radius of a circular search window used to calculate the sum of the greenspace area to detect large greenspaces. Consequently, increasing cooling distance corresponded to a growing abundance of greenspaces classified as large, defined by size over 2 ha, which in the case of the three towns considered here meant that all patches of grass or trees were classed as large for the 200 and 300 m distances ([Fig. 3 Supplementary Materials](#)). Nevertheless, large greenspaces determined by models run for the 100 m cooling distance were realistically distributed across the three towns, assuring validity of the presented results.

The differences in the HMI due to various model parameterisation explored in this study are easily discernible visually ([Fig. 4](#) and Figs. 1–3 in [Supplementary Materials](#)). Maps created for the 100 m cooling distance away from large greenspaces depict lower HMI values in buildings and paved areas than maps generated with larger cooling distances displaying greater variability of HMI values within those LC classes. The sharper delineations of the HMI at 100 m than 200 or 300 m distances are resultant from the overestimation of the abundance of large greenspaces by the model ([Fig. 4 Supplementary Materials](#)). Whilst maps at 2 m resolution generated with 100 m cooling distance showed very little

variation in HMI values within areas covered by grey infrastructure as compared to the 2 m resolution LST map, resampling to 30 m resulted in a greater variability of the HMI values and an overall greater resemblance to the LST map at this resolution. HMI maps generated with 200 m and 300 m cooling distances appeared similar regardless of spatial resolution, however, depicting a lower contrast in HMI values between green, blue and grey LC with increasing cooling distance. Moreover, inclusion of cooling capacity of water bodies in the calculation of the HMI significantly increased their resemblance to LST maps at all cooling distances and spatial resolutions by increasing its values in areas corresponding to low LST of water bodies. Finally, portions of the HMI maps extending beyond the built-up area boundaries marking the area subjected to the regression analysis depicted high heat mitigation values, which corresponded well to the lower observed LST in maps at 30 m resolution. Inclusion of the LC data margin extending beyond the built-up area boundary in the model runs allowed for quantification of cooling effects of the vegetation growing in the rural background of the towns.

### 3.1.2. Assessment within individual LC types

Analysis of  $R^2$  values obtained from the comparison between spatially distributed HMI and LST values, summarised by LC type ([Fig. 5](#) and [Tables 3–5 Supplementary Materials](#)) revealed more complex trends of associations than in the city-wide assessments. First of all, the strength of associations varied simultaneously with LC type and spatial resolution as comparisons at 2 m resolution yielded higher  $R^2$  values for buildings, paved and grass than for trees and water whilst the opposite was true for the 30 m resolution, where HMI for trees appeared to have a stronger association with LST than that for buildings, paved and grass. Moreover,  $R^2$  differed also with the cooling distance of large greenspaces with the highest  $R^2$  for buildings and paved classes observed for distance of 200 m at 2 m spatial resolution as well as at 30 m resolution for buildings in Luton, with the HMI for the remaining LC classes having the strongest relationship to LST at 100 m cooling distance. Inclusion of cooling capacity of water into the assessment increased the strength of the relationship between HMI and LST in all LC classes at 30 m resolution in Bedford and Milton Keynes and had no effect in Luton. At 2 m resolution, small improvements in  $R^2$  were observed in all LC classes apart from water in Bedford and Milton Keynes.

### 3.2. Changes of LST due to changes in the HMI

Validation of the HMI revealed that it most accurately represented LST after resampling to 30 m resolution with model parameterisation

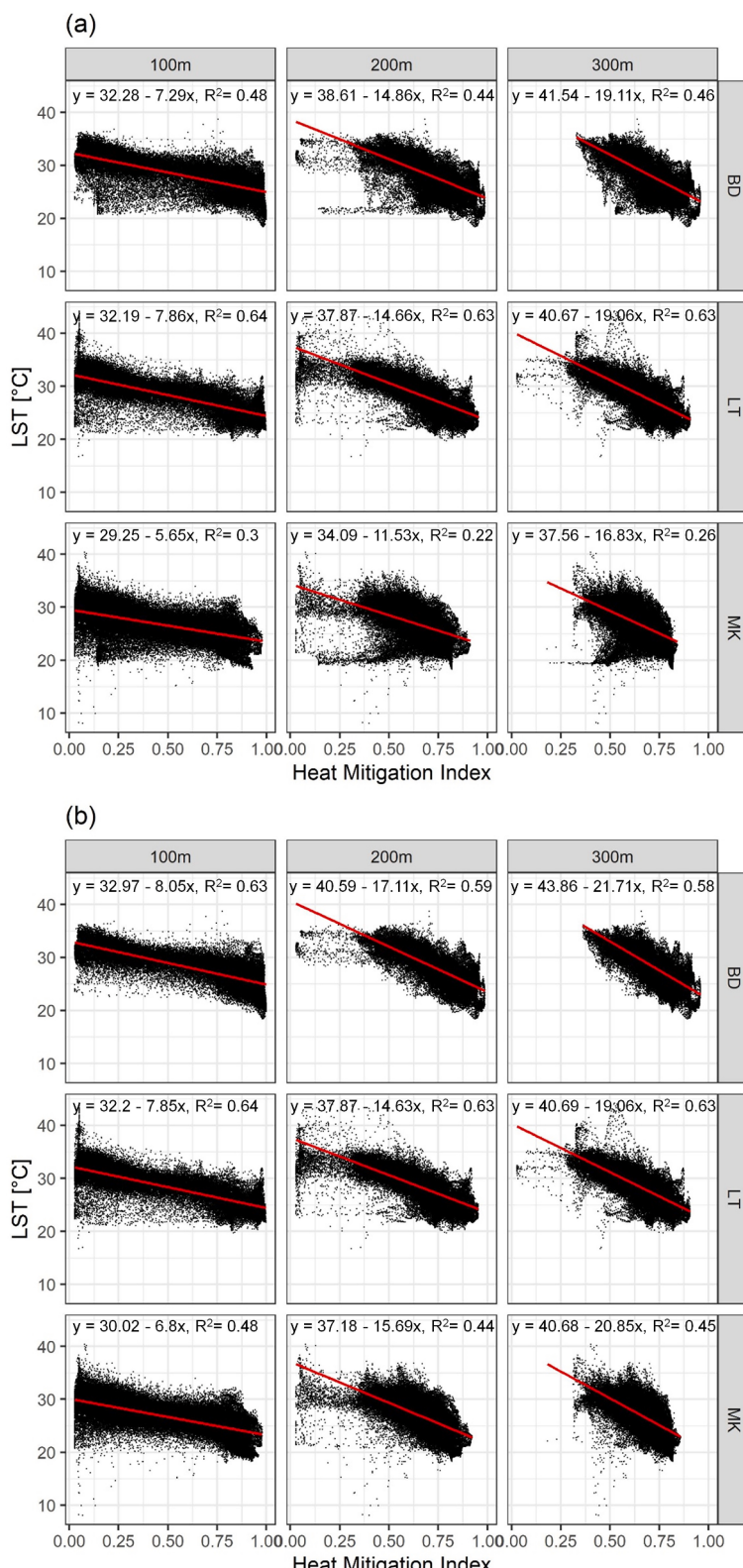


**Fig. 3.** Results of OLS regression between the HMI and LST at 30 m resolution for models (a) excluding and (b) including cooling capacity of water.

including water as a cooling feature and when the 100 m cooling distance away from large vegetated patches was considered. Consequently, linear regression equations obtained from the comparison for these parameters were used to calculate the amount of change in LST due to gradual change in the HMI for all three towns and LC types (Table 4). On average, across all towns, the change in LST due to 0.1 change in the

HMI was 0.76 °C, with the largest change of 0.96 °C attributed to water, followed by trees (app. 0.9 °C), and lowest amount of change occurring within paved (0.65 °C). Differences in observed changes in LST could be attributed to the range of LST values observed within the LC types in each town, with lower ranges of LST yielding a smaller degree of change (Fig. 4 Supplementary Materials).

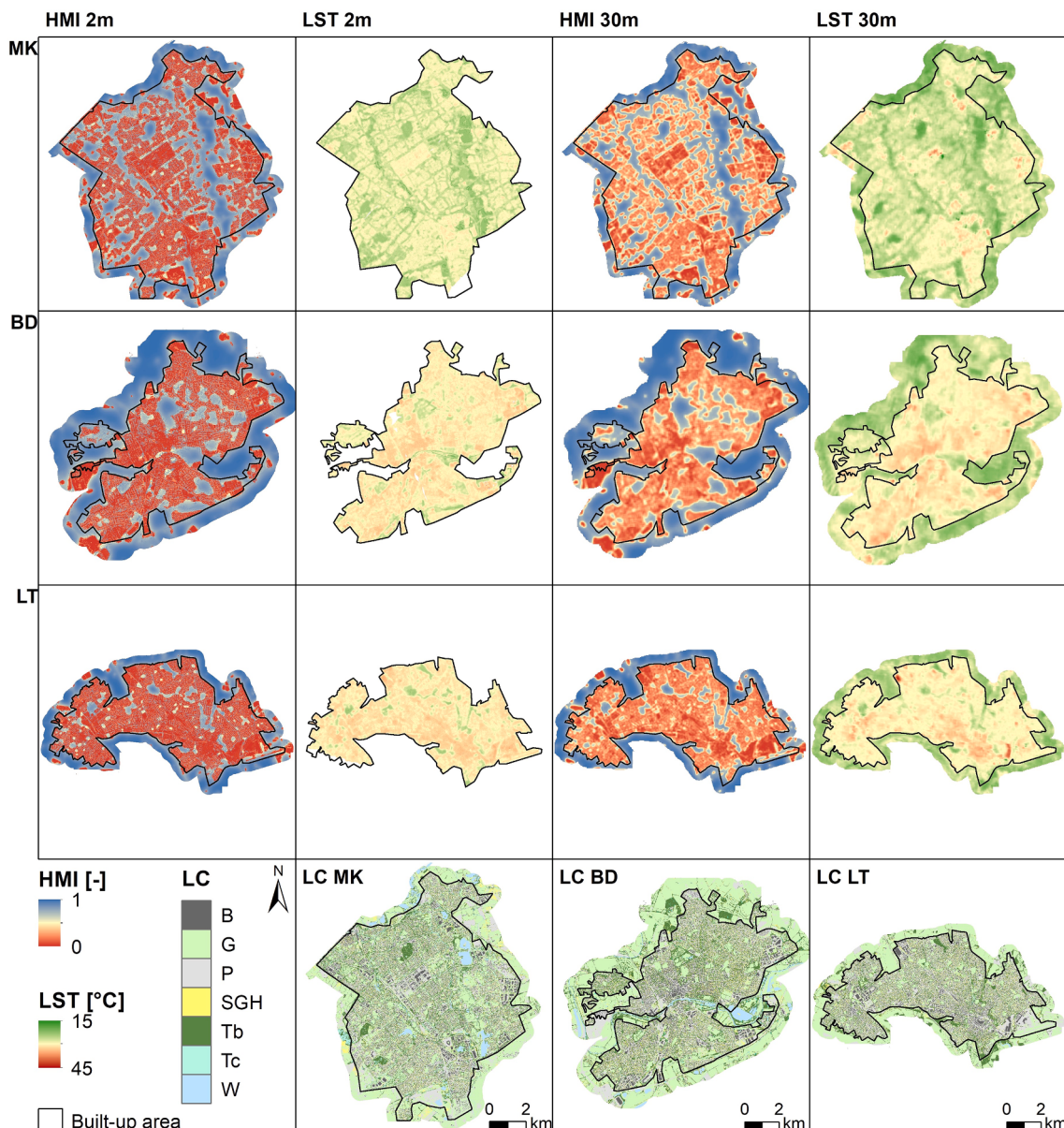


**Fig. 4.** Heat mitigation index (HMI) maps at 2 m and 30 m resolution for Milton Keynes (MK), Bedford (BD) and Luton (LT) at 100 m cooling distance and both vegetation and water set as cooling features. Land surface temperature (LST) at 2 m and 30 m resolution as well as 2 m resolution land cover maps (LC) are shown for comparison and interpretation purposes. Whilst the regression between the HMI and LST maps was carried out for the extent of the built-up boundary only, the Urban Cooling model was run over the entire available extent of the LC data, accounting for any thermal effects exerted by the rural background on the built-up area of the towns.

#### 4. Discussion

The InVEST 3.8.7 Urban Cooling model is aimed at describing the cooling capacity of urban greenspaces on air temperature at their location as well as at a distance away and opens possibilities for testing thermal effects of diverse urban form patterns, such as for example in (Ronchi, Salata, & Arcidiacono, 2020), on excess heat mitigation without carrying out on-site measurements or complex analyses of remotely sensed thermal data, and, at the same time, enabling analysis of synergies and trade-offs between other ecosystem services supplied by these greenspaces. The model incorporates information on key properties of land surface that have been shown to determine air and surface temperatures, and these include evaporative cooling of vegetation, shading by tall trees, and albedo. Whilst consideration of these factors by the model yielded HMI that represented some trends in LST, as demonstrated by the inverse relationship in linear regression, there was

40 to 50% of variation in LST across the three towns, as determined by regression coefficients, that remained unexplained. It has to be noted here that we only used an LST image representing a warm summer day conditions captured at approximately 11 a.m. and the strength of the relationship could be different for LST captured later during the day or a heatwave, when the surface temperature is expected to be higher. There are several further factors that could have influenced the strength of the observed relationship between LST and the HMI and these are discussed below.

Firstly, our approach focussed on the determination of the effects of the cooling distance and spatial resolution of the model outputs without calibration of the weights that are given to albedo, evapotranspiration and shading in the calculation of cooling capacity of urban greenspaces. Whilst InVEST Urban Cooling model calibration carried out by Bosch et al. (2020) over 100 permutations yielded weights that very closely approximated the model default values of 0.2, 0.2 and 0.6 respectively,

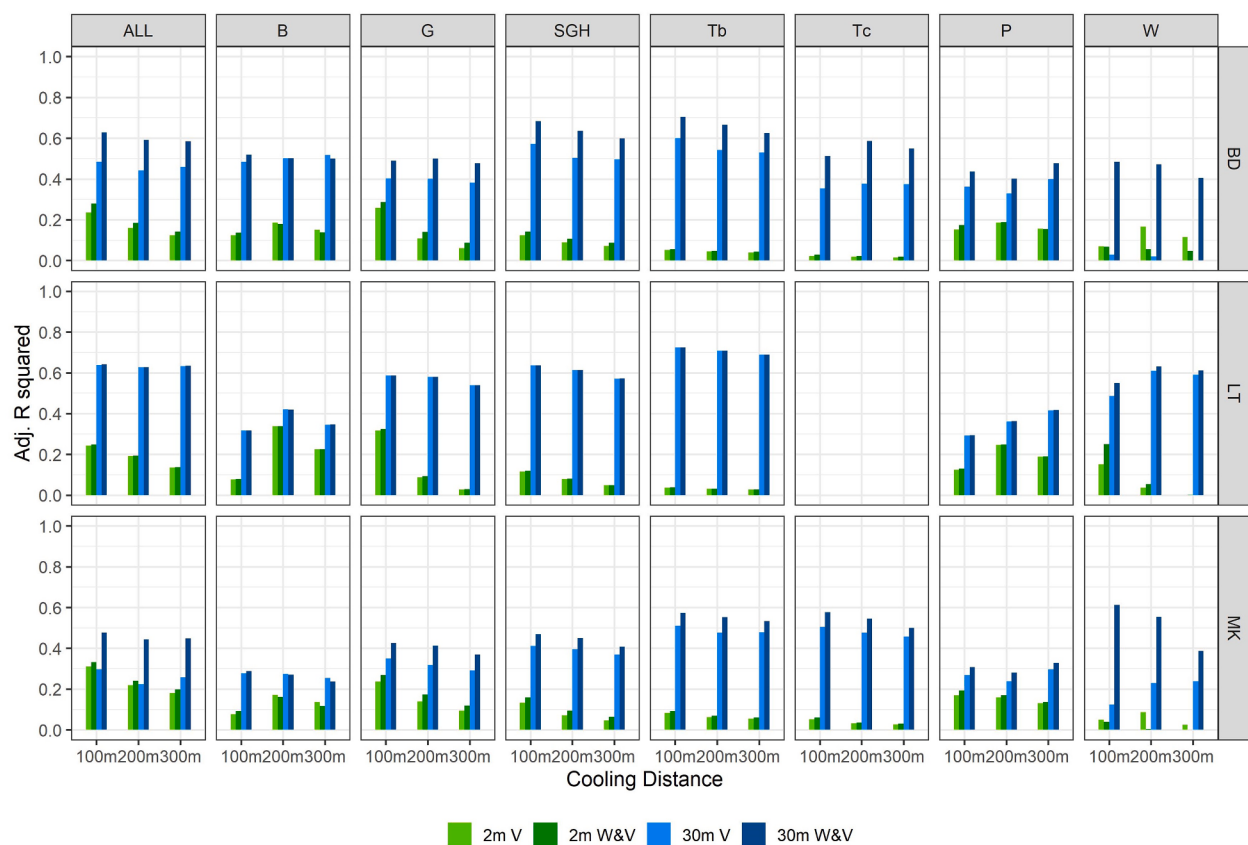


**Fig. 5.** Adjusted R squared values obtained from ordinary least squares regression between HMI and LST values at 2 m (green) and 30 m (blue) resolutions with cooling features set as vegetation (V) or vegetation and water (W&V) and three different cooling distances of large greenspaces for ALL as well as individual land cover classes. B – buildings, G – grass, P – paved, SGH – short trees/tall grass/hedge, Tb – broadleaf trees, Tc – coniferous trees, W – water. (For interpretation of the references to colour in this figure legend, the reader is referred to the web version of this article.)

**Table 4**

The amount of change in LST due to 0.1 change in the HMI for ALL and separate LC types in each town derived with inclusion of cooling capacity of water and cooling distance away from large greenspaces of 100 m, resampled to 30 m resolution. B – buildings, G – grass, P – paved, SGH – short trees/tall grass/hedge, Tb – broadleaf trees, Tc – coniferous trees, W – water.

Town	LC	Change in LST [°C]	Average change [°C]	Std [°C]
BD		0.81		
LT	ALL	0.78	0.76	0.07
MK		0.68		
BD		0.76		
LT	B	1.05	0.88	0.15
MK		0.82		
BD		0.81		
LT	G	0.75	0.72	0.10
MK		0.61		
BD		0.64		
LT	P	0.72	0.65	0.07
MK		0.58		
BD		0.82		
LT	SGH	0.79	0.76	0.08
MK		0.66		
BD		0.99		
LT	Tb	0.93	0.91	0.08
MK		0.82		
BD		0.99		
LT	Tc	–	0.90	0.12
MK		0.81		
BD		0.88		
LT	W	0.84	0.96	0.18
MK		1.17		

these weights should be modified to account for specific climatic or weather conditions affecting a given study area. Evaporative cooling of vegetation in regions experiencing large precipitation, such as for example South East Asia, is of lesser importance and UHI mitigation strategies should focus on maximising shading and ventilation (Manoli et al., 2019). Conversely, the weight for evaporative cooling should be reduced under the expectation of water stress, induced by prolonged hot weather, causing plants to close their stomata, bringing transpiration to a halt (Włoczyk, Borg, Richter, & Miegel, 2011).

Inclusion of water as a cooling feature provided a small improvement in the strength of the relationship between HMI and LST data, especially in Milton Keynes characterised with a higher abundance of water bodies. The role of blue infrastructure in the reduction of the UHI effect is well recognised (Hathway & Sharples, 2012; Peng et al., 2020; Yu et al., 2020) and consequently inclusion of evaporation from water could be considered by the model user, especially when the objective of a study is to estimate air temperatures across a city under non-heat stress weather conditions rather than to quantify the ecosystem service of temperature regulation from vegetation only.

Cooling distance of large greenspaces was another factor that impacted HMI magnitudes and its strength of the relationships with the LST data. Whilst some of the observed differences in HMI driven from different cooling extents of large vegetated patches were expected, it is important to note that the model uses the cooling distance set by the user as the radius of the circular moving window within which the total area of greenspaces is calculated and assigned to each grid cell of the LC map submitted to the model. Consequently, the amount of greenspace considered as large (>2ha in size) will increase with the increasing cooling distance, resulting in an unrealistic representation of the HMI, which in the case of this study manifested in decreasing  $R^2$  values for

200 m and 300 m cooling distances. Moreover, the minimum radius of a circle yielding an area of 2 ha is approximately 80 m, meaning that no greenspaces can be classified as large should the model be run for cooling distances below that value, reducing the interpretation of the heat mitigation index to the cooling capacity as presented in Equation 1 by limiting the heat mitigation capacity of greenspaces to their footprints only. Given that some authors identified the cooling distance of urban parks or water bodies to be <80 m (Broadbent, Coutts, Tapper, Demuzere, & Beringer, 2018; Motazedian, Coutts, & Tapper, 2020), this could potentially weaken the accuracy of the model's air temperature estimates calculated based on the heat mitigation index. This instability of the model could be resolved in future releases by separating the cooling distance setting from the size of the search window within which to calculate the amount of greenspace, allowing for parameterisation of the model to better represent specific morphologies of different towns.

Whilst at 30 m resolution surface temperature of greenspaces was generally well represented by the HMI, some improvement could be made for buildings and paved areas. This is especially important in the context of the Urban Cooling model's capacity to assess the economic value of vegetative cooling by considering energy savings due to decreased use of air conditioning requiring accurate heat mitigation estimates for buildings. The Urban Cooling model attempts at representation temperature of grey infrastructure through the interplay of albedo and cooling capacity of large greenspaces at a distance away. Albedo, which corresponds to the amount of solar radiation reflected and therefore not absorbed by the land surface, manifests in the visible light spectrum as the brightness of colour, which can be captured through analysis of multispectral aerial or satellite remotely sensed data, allowing for diversification of its values within paved areas and buildings (Ejiagha et al., 2020; Hofierka, Gallay, Onačillová, & Hofierka, 2020). Moreover, LST of urban land cover is affected not only by albedo, but also the spatial properties of individual land cover patches, as demonstrated by W. Zhou, Huang, & Cadenasso (2011), which is further confirmed by variable HMI magnitudes obtained in this study for towns with different morphologies. Adaptation of the input LC map for differences in albedo as well as spatial properties of land cover classes could offer a possibility for improvement in representation of their temperature by the HMI, however, these would involve a more sophisticated approach to data preparation requiring extensive expertise in spatial data analysis that may not be available for all model users (Norton et al., 2015). Additionally, Trlica, Hutyra, Schaaf, Erb, & Wang, (2017) have shown that clear relationships between albedo and LST can be obtained after averaging of 30 m resolution data up to 500 m, which corresponds well with the radius of the Gaussian filter kernel suggested by InVEST Urban Cooling model developers to derive air temperature from the HMI, and implying that greater diversification of albedo values submitted to the model might be spurious.

Another factor reducing the strength of the relationship between the HMI and LST could involve the fact that the Urban Cooling model does not make an account of shading provided by buildings – an effect that can provide significant cooling especially within urban canyons appropriately oriented to the direction of incoming solar radiation (Chen et al., 2020). Furthermore, the date stamps of LST imagery and land cover maps used in this study are somewhat offset in time, with the LST maps having been captured approximately one and a half years later than the topographic maps from which the distribution of buildings and paved areas were derived. Whilst the time difference is not large, it could have resulted in some discrepancies between land cover and LST at the outskirts of the towns where new development is likely to take place.

The magnitudes of the HMI and the outcomes of the comparison to LST data were impacted by the spatial resolution of the datasets used in the assessment. Whilst associations between these HMI and LST at 2 m resolution, corresponding to the spatial resolution of the input LC map, were modest to low, they gained in strength after resampling of the HMI to match the mixed 30 m resolution of Landsat-8 derived LST map – an effect that was observed in both the city-wide and individual LC class

assessments. This varied behaviour could be an indicator of an under-representation of the natural variation of LST by the HMI within each LC class in 2 m resolution outputs, which was mitigated through the resampling procedure to 30 m that captured responses from different LC classes into each coarser resolution grid cell through introduction of mixed pixels (Yow, 2007).

Furthermore, as demonstrated by higher comparability of coarse resolution HMI and LST datasets, the model outputs are more suitable for broader assessments that are equivalent to neighbourhood or city scales as suggested by Parsaei et al. (2019) and can therefore support decisions aimed at mitigation of the surface urban heat island at the master plan level. This is especially true given that the relationship between LST and air temperature in urban areas is weak at very fine resolutions of the LST data, with LST hotspots not necessarily coinciding with hotspots in air temperature (Coutts et al., 2016). This relationship, however, strengthened upon coarsening the spatial resolution of the LST images and supported the conclusion of this study of limited suitability of the HMI for micro-scale city planning.

## 5. Conclusions

In this study, the heat mitigation index generated by the InVEST 3.8.7 Urban Cooling model was validated by comparison to land surface temperature images captured on a warm summer day at two spatial resolutions: 2 and 30 m in three sub-urban towns. The results suggested that the index is capable of depicting a portion of the thermal response of land surface, especially for towns with a denser built-up structure and at a coarser spatial resolution, making the model suitable for studies at the masterplan level. Future work should consider testing the model under different heat scenarios that may affect the evaporative capacity of the vegetation as well as the possibility of diversification of not only the weights for shading, evapotranspiration and albedo but also the input LC maps according to internal variability of these factors within each LC type. This study has also demonstrated that the inclusion of evaporation from water bodies in the cooling capacity calculations can improve the accuracy of the heat mitigation index computed by the model, especially in cities with higher abundance of water bodies, indicating that cooling capacity of water can be successfully represented by the model.

We found one important limitation of the model affecting the definition of large greenspaces and their cooling capacity estimates beyond their footprints, related to the entanglement of the cooling distance setting with the radius of the search window used to identify large greenspaces. Whilst the 100 m cooling distance in this study returned heat mitigation index with the highest resemblance to land surface temperature data as well as a realistic representation of large greenspaces, the use of cooling distances lower than 80 m or higher than 100 m would result in under- and over-representation of large greenspaces and their cooling capacity, potentially leading to an erroneous estimation of the value of local temperature regulation ecosystem service by urban greenspaces or misidentification of urban form patterns conducive to cooler air temperatures in the cities. Consequently, authors should take extra care when selecting the cooling distances of large greenspaces to assure that the model represents their abundance well within their study areas, ensuring high accuracy of the heat mitigation estimates returned by the model.

## Acknowledgements

This research (Grant Number NE/J015067/1) was conducted as part of the Fragments, Functions and Flows in Urban Ecosystem Services (F3UES) project as part of the larger Biodiversity and Ecosystem Service Sustainability (BESS) framework. BESS is a six-year programme (2011–2017) funded by the UK Natural Environment Research Council (NERC) and the Biotechnology and Biological Sciences Research Council (BBSRC) as part of the UK's Living with Environmental Change (LWEC) programme. This work presents the outcomes of independent research

funded by NERC and the BESS programme, and the views expressed are those of the authors and not necessarily those of the BESS Directorate or NERC. Additionally, authors would like to thank the anonymous reviewers for their insightful comments that helped shape the final version of this manuscript.

## Appendix A. Supplementary data

Supplementary data to this article can be found online at <https://doi.org/10.1016/j.landurbplan.2021.104163>.

## References

- Aleksandrowicz, O., Vuckovic, M., Kiesel, K., & Mahdavi, A. (2017). Current trends in urban heat island mitigation research: Observations based on a comprehensive research repository. *Urban Climate*, 21, 1–26. <https://doi.org/10.1016/j.jclim.2017.04.002>.
- Allen, R. G., Pereira, L. S., Raes, D., & Smith, M. (1998). Crop evapotranspiration—Guidelines for computing crop water requirements—FAO Irrigation and drainage paper 56. Retrieved from. <https://www.researchgate.net/publication/235704197>.
- Aram, F., Higueras García, E., Solgi, E., & Mansournia, S. (2019). Urban green space cooling effect in cities. *Heliyon*, 5(4), Article e01339. <https://doi.org/10.1016/j.heliyon.2019.e01339>.
- Bherwani, H., Singh, A., & Kumar, R. (2020). Assessment methods of urban microclimate and its parameters: A critical review to take the research from lab to land. *Urban Climate*, 34, Article 100690. <https://doi.org/10.1016/j.jclim.2020.100690>.
- Bosch, M., Locatelli, M., Hamel, P., Remmeh, R., Chenal, J., & Joost, S. (2020). A spatially-explicit approach to simulate urban heat islands in complex urban landscapes. *Geoscientific Model Development Discussions*, 1–22. <https://doi.org/10.5194/gmd-2020-174>.
- Bowler, D. E., Buyung-Ali, L., Knight, T. M., & Pullin, A. S. (2010). Urban greening to cool towns and cities: A systematic review of the empirical evidence. *Landscape and Urban Planning*, 97(3), 147–155. <https://doi.org/10.1016/j.landurbplan.2010.05.006>.
- Broadbent, A. M., Coutts, A. M., Tapper, N. J., Demuzere, M., & Beringer, J. (2018). The microscale cooling effects of water sensitive urban design and irrigation in a suburban environment. *Theoretical and Applied Climatology*, 134(1–2), 1–23. <https://doi.org/10.1007/s00704-017-2241-3>.
- Casanueva, A., Kotlarski, S., Fischer, A. M., Flouris, A. D., Kjellstrom, T., Lemke, B., ... Liniger, M. A. (2020). Escalating environmental summer heat exposure—a future threat for the European workforce. *Regional Environmental Change*, 20(2), 1–14. <https://doi.org/10.1007/s10113-020-01625-6>.
- Chen, G., Wang, D., Wang, Q., Li, Y., Wang, X., Hang, J., ... Wang, K. (2020). Scaled outdoor experimental studies of urban thermal environment in street canyon models with various aspect ratios and thermal storage. *Science of the Total Environment*, 726, Article 138147. <https://doi.org/10.1016/j.scitotenv.2020.138147>.
- Cortinovis, C., & Geneletti, D. (2019). A framework to explore the effects of urban planning decisions on regulating ecosystem services in cities. *Ecosystem Services*, 38, Article 10046. <https://doi.org/10.1016/j.ecoser.2019.100946>.
- Coutts, A. M., Harris, R. J., Phan, T., Livesley, S. J., Williams, N. S. G., & Tapper, N. J. (2016). Thermal infrared remote sensing of urban heat: Hotspots, vegetation, and an assessment of techniques for use in urban planning. *Remote Sensing of Environment*, 186, 637–651. <https://doi.org/10.1016/j.rse.2016.09.007>.
- Droogers, P., & Allen, R. G. (2002). Estimating reference evapotranspiration under inaccurate data conditions. *Irrigation and Drainage Systems*, 16(1), 33–45. <https://doi.org/10.1023/A:1015508322413>.
- Ejiajha, I. R., Ahmed, M. R., Hassan, Q. K., Dewan, A., Gupta, A., & Rangelova, E. (2020). Use of Remote Sensing in Comprehending the Influence of Urban Landscape's Composition and Configuration on Land Surface Temperature at Neighbourhood Scale. *Remote Sensing*, 12(15), 2508. <https://doi.org/10.3390/rs12152508>.
- Elliott, H., Eon, C., & Breadsell, J. K. (2020). Improving City Vitality through Urban Heat Reduction with Green Infrastructure and Design Solutions: A Systematic Literature Review. *Buildings*, 10(12), 219. <https://doi.org/10.3390/buildings10120219>.
- Erell, E. (2008). The Application of Urban Climate Research in the Design of Cities. *Advances in Building Energy Research*, 2(1), 95–121. <https://doi.org/10.3763/aber.2008.0204>.
- European Commission. (2013). Building a green infrastructure for Europe - Publications Office of the EU. <https://doi.org/doi.org/10.2779/54125>.
- Graffius, D. R., Corstanje, R., Siriwardena, G. M., Plummer, K. E., & Harris, J. A. (2017). A bird's eye view: Using circuit theory to study urban landscape connectivity for birds. *Landscape Ecology*, 32(9), 1771–1787. <https://doi.org/10.1007/s10980-017-0548-1>.
- Graffius, D. R., Corstanje, R., Warren, P. H., Evans, K. L., Hancock, S., & Harris, J. A. (2016). The impact of land use/land cover scale on modelling urban ecosystem services. *Landscape Ecology*, 31(7), 1509–1522. <https://doi.org/10.1007/s10980-015-0337-7>.
- Graffius, D. R., Corstanje, R., Warren, P. H., Evans, K. L., Norton, B. A., Siriwardena, G. M., ... Harris, J. A. (2019). Using GIS-linked Bayesian Belief Networks as a tool for modelling urban biodiversity. *Landscape and Urban Planning*, 189, 382–395. <https://doi.org/10.1016/j.landurbplan.2019.05.012>.
- Gunawardena, K. R., Wells, M. J., & Kershaw, T. (2017). Utilising green and bluespace to mitigate urban heat island intensity. *Science of the Total Environment*, 584–585, 1040–1055. <https://doi.org/10.1016/j.scitotenv.2017.01.158>.
- Hathaway, E. A., & Sharples, S. (2012). The interaction of rivers and urban form in mitigating the Urban Heat Island effect: A UK case study. *Building and Environment*, 58, 14–22. <https://doi.org/10.1016/j.buildenv.2012.06.013>.
- Heaviside, C., Macintyre, H., & Vardoulakis, S. (2017). The Urban Heat Island: Implications for Health in a Changing Environment. *Current Environmental Health Reports*, 4(3), 296–305. <https://doi.org/10.1007/s40572-017-0150-3>.
- Heaviside, C., Vardoulakis, S., & Cai, X.-M. (2016). Attribution of mortality to the urban heat island during heatwaves in the West Midlands. *UK Environmental Health*, 15 (S1), S27. <https://doi.org/10.1186/s12940-016-0100-9>.
- Hofierka, J., Gallay, M., Onácilová, K., & Hofierka, J. (2020). Physically-based land surface temperature modeling in urban areas using a 3-D city model and multispectral satellite data. *Urban Climate*, 31, Article 100566. <https://doi.org/10.1016/j.jclim.2019.100566>.
- Jimenez-Munoz, J. C., Sobrino, J. A., Skokovic, D., Mattar, C., & Cristobal, J. (2014). Land surface temperature retrieval methods from landsat-8 thermal infrared sensor data. *IEEE Geoscience and Remote Sensing Letters*, 11(10), 1840–1843. <https://doi.org/10.1109/LGRS.2014.2312032>.
- Kjellstrom, T., Freyberg, C., Lemke, B., Otto, M., & Briggs, D. (2018). Estimating population heat exposure and impacts on working people in conjunction with climate change. *International Journal of Biometeorology*, 62(3), 291–306. <https://doi.org/10.1007/s00484-017-1407-0>.
- Kleerekooper, L., van Esch, M., & Salcedo, T. B. (2012). How to make a city climate-proof, addressing the urban heat island effect. *Resources, Conservation and Recycling*, 64, 30–38. <https://doi.org/10.1016/j.resconrec.2011.06.004>.
- Lin, P., Gou, Z., Lau, S., & Qin, H. (2017). The Impact of Urban Design Descriptors on Outdoor Thermal Environment: A Literature Review. *Energies*, 10(12), 2151. <https://doi.org/10.3390/en10122151>.
- Manoli, G., Fatichi, S., Schläpfer, M., Yu, K., Crowther, T. W., Meili, N., ... Bou-Zeid, E. (2019). Magnitude of urban heat islands largely explained by climate and population. *Nature*, 573(7772), 55–60. <https://doi.org/10.1038/s41586-019-1512-9>.
- Meng, C. (2017). Mitigating the surface urban heat island: Mechanism study and sensitivity analysis. *Asia-Pacific Journal of Atmospheric Sciences*, 53(3), 327–338. <https://doi.org/10.1007/s13143-017-0036-1>.
- Met Office, Hollis, D., McCarthy, M., Kendon, M., Legg, T., Simpson, I. (2019). HadUK-Grid Gridded Climate Observations on a 1km grid over the UK, v1.0.1.0 (1862–2018). Centre for Environmental Data Analysis, 14 November 2019. <https://doi.org/10.5285/d13435808894b2bb249e9f222c2ec8>.
- Millennium Ecosystem Assessment. (2005). *Ecosystems and Human Well-being: Synthesis*. Washington, DC: Island Press.
- Motazedian, A., Coutts, A. M., & Tapper, N. J. (2020). The microclimatic interaction of a small urban park in central Melbourne with its surrounding urban environment during heat events. *Urban Forestry and Urban Greening*, 52, Article 126688. <https://doi.org/10.1016/j.ufug.2020.126688>.
- Norton, B. A., Coutts, A. M., Livesley, S. J., Harris, R. J., Hunter, A. M., & Williams, N. S. G. (2015). Planning for cooler cities: A framework to prioritise green infrastructure to mitigate high temperatures in urban landscapes. *Landscape and Urban Planning*, 134, 127–138. <https://doi.org/10.1016/j.landurbplan.2014.10.018>.
- Oke, T. R. (1976). The distinction between canopy and boundary-layer urban heat islands. *Atmosphere*, 14(4), 268–277. <https://doi.org/10.1080/00046973.1976.9648422>.
- Oke, T. R. (1988). The urban energy balance. *Progress in Physical Geography*, 12(4), 471–508. <https://doi.org/10.1177/030913338001200401>.
- Oke, T. R., Johnson, G. T., Steyn, D. G., & Watson, I. D. (1991). Simulation of surface urban heat islands under "ideal" conditions at night part 2: Diagnosis of causation. *Boundary-Layer Meteorology*, 56(4), 339–358. <https://doi.org/10.1007/BF00119211>.
- Parsaei, M., Joybari, M. M., Mirzaei, P. A., & Haghhighat, F. (2019). May 1). Urban heat island, urban climate maps and urban development policies and action plans. *Environmental Technology and Innovation*, 14, Article 100341. <https://doi.org/10.1016/j.eti.2019.100341>.
- Perkins, S. E., Alexander, L. V., & Nairn, J. R. (2012). Increasing frequency, intensity and duration of observed global heatwaves and warm spells. *Geophysical Research Letters*, 39(20), 2012GL053361. <https://doi.org/10.1029/2012GL053361>.
- Peng, J., Liu, Q., Xu, Z., Lyu, D., Du, Y., Qiao, R., & Wu, J. (2020). How to effectively mitigate urban heat island effect? A perspective of waterbody patch size threshold. *Landscape and Urban Planning*, 202, 103873. <https://doi.org/10.1016/j.landurbplan.2020.103873>.
- Phelan, P. E., Kaloush, K., Miner, M., Golden, J., Phelan, B., Silva, H., & Taylor, R. A. (2015). Urban Heat Island: Mechanisms, Implications, and Possible Remedies. *Annual Review of Environment and Resources*, 40(1), 285–307. <https://doi.org/10.1146/annurev-environ-102014-021155>.
- Ronchi, S., Salata, S., & Arcidiacono, A. (2020). Which urban design parameters provide climate-proof cities? An application of the Urban Cooling InVEST Model in the city of Milan comparing historical planning morphologies. *Sustainable Cities and Society*, 63, Article 102459. <https://doi.org/10.1016/j.scs.2020.102459>.
- Roth, M., Oke, T. R., & Emery, W. J. (1989). Satellite-derived urban heat islands from three coastal cities and the utilization of such data in urban climatology. *International Journal of Remote Sensing*, 10(11), 1699–1720. <https://doi.org/10.1080/01431168908904002>.
- Santamouris, M., Cartalis, C., Synnefa, A., & Kolokotsa, D. (2015). On the impact of urban heat island and global warming on the power demand and electricity consumption of buildings—A review. *Energy and Buildings*, 98, 119–124. <https://doi.org/10.1016/j.enbuild.2014.09.052>.

- Sharp, R., Douglass, J., Wolny, S., Arkema, K., Bernhardt, J., Bierbower, W., ... Wyatt, K. (2020). *InVEST 3.8.7.post12+ug.gbcad34f User's Guide. The Natural Capital Project*. Stanford University, University of Minnesota, The Nature Conservancy, and World Wildlife Fund.
- Sung, C. Y. (2013). Mitigating surface urban heat island by a tree protection policy: A case study of The Woodland, Texas, USA. *Urban Forestry & Urban Greening*, 12(4), 474–480. <https://doi.org/10.1016/j.ufug.2013.05.009>.
- Taha, H., Akbari, H., Rosenfeld, A., & Huang, J. (1988). Residential cooling loads and the urban heat island—the effects of albedo. *Building and Environment*, 23(4), 271–283. [https://doi.org/10.1016/0360-1323\(88\)90033-9](https://doi.org/10.1016/0360-1323(88)90033-9).
- Trlica, A., Hutyra, L. R., Schaaf, C. L., Erb, A., & Wang, J. A. (2017). Albedo, Land Cover, and Daytime Surface Temperature Variation Across an Urbanized Landscape. *Earth's Future*, 5(11), 1084–1101. <https://doi.org/10.1002/2017EF000569>.
- Tsoka, S., Tsikaloudaki, K., Theodosiou, T., & Bikas, D. (2020). Urban warming and cities' microclimates: Investigation methods and mitigation strategies—A review. *Energies*, 13(6), 1414. <https://doi.org/10.3390/en13061414>.
- United Nations, Department of Economic, & Social Affairs. (2019). Population Division. *In World Urbanization Prospects: The 2018 Revision (ST/ESA/SER.A/420)*. New York: United Nations.
- Vaz Monteiro, M., Doick, K. J., Handley, P., & Peace, A. (2016). The impact of greenspace size on the extent of local nocturnal air temperature cooling in London. *Urban Forestry and Urban Greening*, 16, 160–169. <https://doi.org/10.1016/j.ufug.2016.02.008>.
- Voogt, J., & Oke, T. (2003). Thermal remote sensing of urban climates. *Remote Sensing of Environment*, 86(3), 370–384. [https://doi.org/10.1016/S0034-4257\(03\)00079-8](https://doi.org/10.1016/S0034-4257(03)00079-8).
- Wang, W., Yao, X., & Shu, J. (2020). Air advection induced differences between canopy and surface heat islands. *Science of The Total Environment*, 725, Article 138120. <https://doi.org/10.1016/j.scitotenv.2020.138120>.
- Wloczyk, C., Borg, E., Richter, R., & Miegel, K. (2011). Estimation of instantaneous air temperature above vegetation and soil surfaces from Landsat 7 ETM+ data in northern Germany. *International Journal of Remote Sensing*, 32(24), 9119–9136. <https://doi.org/10.1080/01431161.2010.550332>.
- Wouters, H., De Ridder, K., Poelmans, L., Willems, P., Brouwers, J., Hosseinzadehtalaei, P., ... Demuzere, M. (2017). Heat stress increase under climate change twice as large in cities as in rural areas: A study for a densely populated midlatitude maritime region. *Geophysical Research Letters*, 44(17), 8997–9007. <https://doi.org/10.1002/2017GL074889>.
- Yow, D. M. (2007). Urban Heat Islands: Observations, Impacts, and Adaptation. *Geography Compass*, 1(6), 1227–1251. <https://doi.org/10.1111/j.1749-8198.2007.00063.x>.
- Yu, Z., Yang, G., Zuo, S., Jørgensen, G., Koga, M., & Vejre, H. (2020). Critical review on the cooling effect of urban blue-green space: A threshold-size perspective. *Urban Forestry & Urban Greening*, 49, 126630. <https://doi.org/10.1016/j.ufug.2020.126630>.
- Zardo, L., Geneletti, D., Pérez-Soba, M., & Van Eupen, M. (2017). Estimating the cooling capacity of green infrastructures to support urban planning. *Ecosystem Services*, 26, 225–235. <https://doi.org/10.1016/j.ecoser.2017.06.016>.
- Zawadzka, J., Corstanje, R., Harris, J., & Truckell, I. (2020). Downscaling Landsat-8 land surface temperature maps in diverse urban landscapes using multivariate adaptive regression splines and very high resolution auxiliary data. *International Journal of Digital Earth*, 13(8), 899–914. <https://doi.org/10.1080/17538947.2019.1593527>.
- Zhou, D., Xiao, J., Bonafoni, S., Berger, C., Deilami, K., Zhou, Y., ... Sobrino, J. A. (2019). Satellite remote sensing of surface urban heat islands: Progress, challenges, and perspectives. *Remote Sensing*, 11, 48. <https://doi.org/10.3390/rs11010048>.
- Zhou, W., Huang, G., & Cadenasso, M. L. (2011). Does spatial configuration matter? Understanding the effects of land cover pattern on land surface temperature in urban landscapes. *Landscape and Urban Planning*, 102(1), 54–63. <https://doi.org/10.1016/j.landurbplan.2011.03.009>.